Precipitation and circulation covariability in the extratropics

René D. Garreaud

(rgarreau@dgf.uchile.cl)

Department of Geophysics. Universidad de Chile.

Submitted to *Journal of Climate* - September 2006

Abstract

Extratropical precipitation is primarly produced by cold and warm fronts associated with surface cyclones and upper-level troughs. The growth of these midlatitude storms is partially controlled by the dry baroclinicity of the troposphere, which in turn can be roughly quantified by the intensity of the upper-level zonal flow. Orographic rainfall, an important component of the precipitation in several midlatitude regions, is also partially determined by the intensity of the cross-mountain mid-level winds. Thus, temporal variations of precipitation and zonal flow aloft at a given location should exhibit some degree of coherence. In this work we document the local covariability of these variables over several time scales, using global precipitation products and atmospheric reanalysis from 1979 to 2004. We also document the spatial correspondence between the precipitation and circulation when considering their climatological annual means.

The local correlation (r_0) between monthly anomalies of precipitation and upper level (300 hPa) zonal flow varies on space, from moderately and even highly significant values ($r_0 \sim 0.3$ to 0.7) over the midlatitude oceans to near zero over the interior of continental areas. Similar results are found when considering the monthly variance of the high-pass-filtered meridional wind (an index of eddy activity) or the annual means of the variables. The local correlation map between precipitation and low-level (850 hPa) zonal flow is similar to its upper-level counterpart, but the correlations over open ocean are somewhat weaker while orographic effects show up more clearly. The correlation are positive and large upstream of the major north-south oriented mountain ranges, as strong westerlies promote upslope rain in addition to storm-related precipitation. In contrast, the correlation tends to be negative downstream of the ranges, as strong westerlies enhance the rain shadow effects over the lee side.

1 Introduction

Tropical and extratropical precipitation are readily differentiated on the basis of the zonal average of annual mean rainfall (e.g., Fig. 1b), because of a marked subtropical minimum found in both hemispheres. Tropical precipitation (within 20° of the equator) accounts for nearly half of the global precipitation and it is mostly produced by convective clouds (deep and shallow) and their associated areas of stratiform clouds. Extratropical precipitation reaches a maximum in midlatitudes (40°-50°), primarily produced by deep stratiform clouds (nimbostratus) and embedded convective cells that develop along cold and warm fronts. The frontal systems are in turn associated with surface cyclones, an integral part of the baroclinic waves that populate the midlatitudes.

Although each midlatitude storm (or transient eddy) exhibits a unique evolution, they tend to move along rather narrow latitudinal bands known as storm tracks (e.g., Hoskins and Valdes 1990), whose identification and diagnosis has been performed using several methods and variables (e.g., Hoskins and Hodges 2002). In the Northern Hemisphere (NH) the prominent storm tracks are located over the midlatitude Atlantic and Pacific oceans, attaining maximum intensity in early winter and fall/spring, respectively (e.g., Nakamura 1992). A secondary NH storm track is found during summer over high-latitude landmasses (e.g., Yoon and Chen 2006). In the Southern Hemisphere (SH) there is a single, subpolar storm track during the austral summer, most intense over the eastern Atlantic and Indian ocean (e.g., Trenberth 1991; Nakamura and Shimpo 2004). During austral winter strong upper-level wave activity is also found at subtropical latitudes stretching from the Indian ocean into the eastern Pacific.

According to the linear theory, the growth of individual eddies is highly dependent on the dry baroclinicity of the large-scale flow in which they evolve (e.g., Frederiksen and Frederiksen 1993). Nevertheless, non-linear effects and diabatic heating complicate the eddy-mean flow relationship. Furthermore, there are several indices of baroclinic eddy activity, between which the correlation is only low to moderate outside the core of the storm tracks (e.g., Paciorek *et al.* 2002). Thus, when considering seasonal or annual means, the correspondence between the position and intensity of, say, upper-level jet streams and storm tracks is not particularly strong (e.g., Chang 2002; Nakamura and Shimpo 2004).

Because of the lack of a direct relation between cyclone intensity and rain formation, the correspondence between circulation and precipitation on seasonal and longer time-scales should be further complicated. Such relation is particularly difficult to establish over subtropical regions, where most of the rainfall is caused by upper-level disturbances and the subtropical end of cold fronts arching equatorward from storms moving at higher latitudes (e.g., Eichler and Higgins 2006). Furthermore, only about half of the cyclones are associated with warm conveyor belts (WCB, Eckhardt *et al.* 2004), one of the primary regions of rain formation on midlatitude storms. On the other hand, some of the rainiest areas in midlatitudes are found in the windward side of major mountain ranges,

where the amount of orographic precipitation is, at least, partially explained by the intensity of the cross-mountain flow at low- and mid-levels (e.g., Roe 2005).

Thus, it is not obvious whether precipitation and zonal flow aloft exhibit coherence in their temporal variations, in which time-scale (if any) the coupling is significant, and how the degree of coupling varies on space. In this work we aim to answer these questions by mapping the local covariability between precipitation and several circulation variables over seasonal, intraseasonal and interannual time-scales. The global precipitation products and atmospheric reanalysis used in our analysis are described in section 2. In section 3 we document the spatial correspondence between the precipitation and the circulation fields when considering their climatological annual means, as well as the covariability on the climatological annual cycle. In section 4 we describe the covariability on intraseasonal (month-to-month) and interannual scales, including topographic and continental effects, as well as the association between large-scale circulation variability and regional-scale precipitation anomalies. Section 5 presents our concluding remarks.

2 Data and methods

Two global datasets have been primarily used in this work: the National Centers for Environmental Prediction - National Center for Atmospheric Research (NCEP-NCAR) Reanalysis (NNR, Kalnay *et al.* 1996) and the Climate Prediction Center (CPC) Merged Analysis of Precipitation (CMAP, Xie and Arkin 1997). Our analysis is based on monthly mean values and extends over 26 years from January 1979 to December 2004. Wind, geopotential height, and relative humidity at isobaric levels were taken from the NCEP-NCAR reanalysis to characterize the tropospheric circulation. CMAP is a widely used precipitation product obtained by merging gauge observations, several satellite estimates and blended NNR precipitation.

To document the precipitation-circulation covariability, we calculated the Pearson (ordinary) correlation between pair of time series (precipitation and circulation) at collocated grid points. The circulation variables include zonal and meridional flow at 300 hPa and 850 hPa (U_{300}, V_{300}, U_{850}, V_{850}, respectively). As an index of the eddy-activity we use the monthly variance of the band-pass-filtered (3-15 days) 300 hPa meridional wind (ΣV_{300}) calculated from daily mean values of V_{300}. Although CMAP and NNR are both on $2.5^\circ \times 2.5^\circ$ lat-lon grid, CMAP data corresponds to the area-mean precipitation at each box (the first box centered at 88.75°S, 1.25°E) while NNR represents variables at the grid's nodes (the first node at 90°S,0°E). Therefore, NNR variables were translated to the center of the boxes by averaging the values at the four surrounding nodes. The local correlation (r_0) was obtained for each of the 10368 (144×72) grid boxes over the globe and displayed on a map if statistically significant. The

significance was assessed locally using a two-tailed Student's t-test at the 95% confidence level.

Because CMAP has spatially varying degrees of uncertainty, all the calculations presented later (sections 3 and 4) were repeated using two alternative dataset of global precipitation: the observation-only CMAP (CMAP/O) and the Global Precipitation Climatology Project (GPCP, Adler *et al.* 2003). CMAP/O does not include reanalysis precipitation and it has no data over oceanic regions poleward of 60° where satellite estimates are considered unreliable (Xie and Arkin 1997). GPCP is also a gridded analysis, that incorporates several satellite precipitation estimates and gauge observations. Yin *et al.* (2004) compared CMAP and GPCP showing that the two products are generally in good agreement, although significant differences were noted in the tropical oceans and high-latitude land areas, and it is not possible to conclude that one product supersedes the other. Nonetheless, the patterns of covariability obtained with CMAP/O and GPCP in the present work (e.g., maps of r_0) are very similar to those obtained with CMAP, and hence our results appear robust with respect to changes in the precipitation dataset.

3 Climatological annual mean and annual cycle

Before we explore the covariability of precipitation and circulation over several time scales, it is worthwhile to document the *spatial* relation between these two variables when considering their climatological annual means. To this end, Fig. 1a displays the long-term annual mean precipitation (P), 300 hPa zonal wind (U_{300}), and variance of 300 hPa meridional wind (ΣV_{300}). When displayed on a map, the distinction between tropical and extratropical precipitation regimes is less evident, since the bands of strong precipitation over the midlatitude oceans are connected with tropical areas of rainfall (South/Central America, equatorial Africa and the maritime continent). The connection is particularly marked in the SH during austral summer, throughout the so called South Pacific and South Atlantic convergence zones (SPCZ and SACZ, respectively).

Broadly speaking, the spatial distribution of annual mean precipitation and upper-level zonal flow tends to agree. In the NH midlatitudes, precipitation is largest in the western side of the Atlantic and Pacific oceans, roughly underneath the corresponding jet stream. In the SH the correspondence is weaker. The poleward flanks of the SPCZ and SACZ are also under strong upper-level winds, but precipitation is relatively modest under the core of the subpolar jet stream in the Indian ocean. Further, the entrance region of the subtropical jet stream resides over the dry western Australia. Also noteworthy is that the midlatitude regions with maximum precipitation are under relatively weak zonal flow: the western coasts of boreal North America and austral South America, New Zealand and Tasmania. Orographic rainfall is a major contribution to the total precipitation over these mountainous regions.

The aforementioned spatial association is conveniently summarized in the scatter plot of the annual mean U_{300} and P shown in Fig. 2a along with the statistical parameters. Extratropical precipitation tends to increase linearly with zonal flow aloft; overall the spatial variability of U_{300} explains nearly 40% of the spatial variability of P. As expected, the slope of the trend is steeper and the scatter is smaller in the NH relative to the SH, indicative of tighter coupling between upper level flow and precipitation in the NH. No significant differences are found when the scatter plot is constructed using climatological seasonal means or when using the other precipitation datasets.

The correspondence between precipitation and 300 hPa meridional wind variance over the extratropics is slightly weaker than when considering U_{300} (Figs. 1a and 2b); considering both the NH and SH extratropics the spatial variability of ΣV_{300} only explains 25% of the spatial variability of P. In the NH the intensity of the storm activity, as gauged by ΣV_{300}, is largest poleward and downstream of the core of the oceanic jet stream and hence, displaced from the precipitation maximum. The variance of V_{300} is also high over the interior of North America and Siberia, where precipitation is modest relative to the oceanic areas. In the SH, most of the discrepancy stems from the low storm activity (annually averaged) over the SPCZ, as well as the relatively modest rainfall around Antarctica underneath the persistent subpolar storm track.

Let us now explore what fraction of the mean annual cycle of precipitation is accounted for its circulation counterpart. Although the amplitude of the mean annual cycle of precipitation in the extratropics is small (typically $<$20% of the annual total), its phase shows coherent spatial patterns, as documented by Chen *et al.* 2004. They showed that precipitation over the midlatitude oceans attains a maximum (minimum) during winter (summer), and attributed this cycle to the seasonally varying convergence of transient water vapor flux. Figure 3 shows the local correlation between P and U_{300} using the long-term monthly means at each grid box. Precipitation and zonal flow are highly correlated ($r_0 > +0.6$) over the NH midlatitude oceans, along the extratropical parts of the SPCZ and SACZ, and around Antarctica. In these regions, the correlation between P and ΣV_{300} is also high and positive (not shown). Thus, for most locations over the midlatitude oceans, the maximum (minimum) precipitation in the course of the year tends to occurs during winter (summer) when upper-level winds and eddy activity are at their highest (lowest).

In contrast, the local correlation between P and U_{300} is negative over most of the tropical belt (25°S-25°N), including the monsoonal regimes of the Americas, Africa and Asia, but excluding a narrow equatorial band over the central Pacific. The area of negative correlation extends poleward over North America and Asia, where the maximum precipitation takes place in summer under relatively weak winds aloft, producing a land-ocean precipitation contrast in the NH midlatitudes. Chen *et al.* (2004) also found such contrast, and attributed its origin to the annual seesaw of the convergence of stationary water vapor flux between the western and eastern half of the oceans.

4 Intraseasonal and interannual variability

a. Local correlations

The local correlation map between precipitation and 300 hPa zonal wind using monthly anomalies is shown in Fig. 4a. (At each grid box, the mean annual cycle was removed using the anomaly filter). Over most of the extratropical oceans, both variables are positively correlated, with anomalies of upper-level zonal flow explaining from 30% to 60% of the precipitation variance on intraseasonal and interannual time scales. In the NH, the local correlations tend to increase eastward over the Atlantic and Pacific oceans. In the SH, there is a belt of large, positive correlations at $\sim$45°S interrupted over eastern South America. High correlations ($r_0 >$ 0.6) are also found along the subtropical portions of the SPCZ and SACZ, and upstream off the west coast of southern South America. In contrast, negative correlations between P and U_{300} are found over the equatorial central Pacific and the equatorial Atlantic. Over the continental land masses, variations of precipitation and zonal flow aloft are mostly uncorrelated. Nevertheless, at least part of the low correlation might stem from the low signal-to-noise ratio over dry continental areas.

The basic interpretation of the positive correlations between precipitation and 300 hPa zonal flow over the midlatitude oceans is that U_{300} is an indicator of the dry baroclinicity of the tropospheric column. Thus, at monthly and longer time scales, strong westerlies aloft are conducive of a rapid growth and fast succession of baroclinic disturbances, leading to an increase of cyclone/frontal precipitation. As discussed in the introduction, however, the previous conceptual sequence is weakly linked so the significant correlation between P and U_{300} is noteworthy. If the local correlations are calculated using seasonal or annual means (not shown) the overall pattern remains similar to that in Fig. 4a, but the absolute values are slightly lower (yet statistically significant) than their counterparts using monthly anomalies. This indicates the relative short time (a month or so) in which zonal flow, eddy activity and precipitation processes are actually coupled.

The increase in local correlation between P and U_{300} near most of the continent's western seabords, relative to the mid-ocean conditions, is likely associated with orographic precipitation processes acting either in concert with or independent of baroclinic storms. Since these processes are more directly controlled by flow near the mountain's ridge level (e.g., Roe 2005), we also constructed the local correlation map between P and U_{850} (Fig. 4b). This map is similar to its upper-level counterpart (c.f. Figs. 4a-b), but for slightly weaker correlations over the oceanic storm tracks and a sign reverse of $r_0$over the tropical belt. The orographic effects, however, does show up more clearly in Fig. 4b. The largest values of r_0 ($>$0.7) are found off the western seabords of South America and North America, as well as upstream of the Iberian and the Scandinavian peninsulas, the British islands and the Siberian Plateau, while bands of significant but *negative* correlation are found on the eastern seabord of Australia, Africa,

and Asia, and the interior of North and South America.

For a north-south oriented mountain range, stronger than normal low-level westerlies increases precipitation in the windward side by enhancing upslope rain. In the lee side there are competing factors. In one hand, stronger than normal westerlies at the mountain top produces more intense downslope flow favoring dry conditions to the east of the ridge (rain shadow effect); on the other hand, enhanced westerlies might increase rainfall by advecting hydrometeors toward the lee slope and increasing the number of baroclinic disturbances moving over the region. At the scale of the present analysis, the enhanced rain shadow effect is dominant, as signaled by the pronounced west-to-east decrease of r_0 (even the change of its sign) observed across the southern Andes, the Rockies, the Great Dividing range, and the Southern Alps, as well as the South Africa Plateau and Greenland. For more east-west oriented topographic features, such as the Antarctica periphery and the gulf of Alaska, the best local correlations between precipitation and circulation are found when considering V_{850} (not shown).

Since the amount of precipitation also depends on the available water supply, several authors have included relative humidity at 850 hPa (RH_{850}) in their statistical downscaling models of precipitation (e.g., Pandey *et al.* 1999). Fig. 5 shows the increase in the variance (Δr^2) of precipitation explained when using U_{850} and RH_{850} as "predictors" on a multi-variable linear fit, relative to the case when only U_{850} is used (i.e., r_0^2). The increase in local correlation over oceanic midlatitudes is modest ($\Delta r^2 \leq 0.1$). In contrast, large values of $\Delta r^2 (> 0.3)$ are found over continental land masses (central Europe and the Siberian plains, central North America, Australia and South Africa), where the correlation $RH_{850} - P$ is positive and large, and the correlation $U_{850} - P$ is very small. Whether low-level moisture variability over those continental areas actually controls precipitation or vice-versa, is open to question and requires further analysis.

A local correlation map was also constructed using ΣV_{300} as the circulation variable (Fig. 4c). In both hemispheres, the area of positive, significant local correlation over midlatitudes extends into the subtropics and encompasses several continental areas (e.g., the east seaboard of North America). The local correlations are, however, lower than their counterparts when using U_{300} despite of the closer conceptual link between precipitation and eddy activity. That is probably a reflection of the more "noisy" (in time and space) character of the variance field. We must emphasize that ΣV_{300} is just one among several indices of eddy activity (e.g., Paciorek *et al.* 2002), and use of another index (e.g., low-level meridional transient heat flux) might yield slightly different results.

b. Spatial Patterns

One may speculate that an increase of U_{300} over one particular grid box should produce not only a local but also a downstream increase in eddy activity and precipitation. To test this, precipitation at each grid box was correlated with U_{300} everywhere; an example of such 1-point correlation map is shown in Fig. 6a for a grid box centered at 40°N-160°W (central North Pacific). In this case,

the maximum correlation (r_{max}) is obtained for a U_{300} grid box that is offset 10° westward and 5° equatorward (about 1400 km away) from the precipitation grid box, but $|r_{max}| - |r_0| \sim 0.1$, a difference below statistical significance. Similar results are found elsewhere: the correlation between precipitation and upper zonal wind does maximize when considering a U_{300} grid box 5-10° to the west of the P grid box, but the increase in correlation is, at the best, marginal.

The 1-point correlation map presented in Fig. 6a also indicates that rainier than normal conditions over the central North Pacific are associated with an elongated area of strong cyclonic anomalies at higher latitudes, and weaker anticyclonic anomalies centered at roughly the same longitude but farther south. Such north-south oriented dipole of geopotential anomalies steepens (or relax) the meridional pressure gradient at midlatitudes, thus increasing (reducing) the zonal flow at 40°N, where P and U_{300} are highly correlated.

To investigate the generality of this pattern, precipitation at each grid box was correlated with 300 hPa geopotential height elsewhere. For reference grid boxes in midlatitudes and where zonal flow and precipitation are (locally) tightly coupled, we obtained similar results to those found for the central North Pacific. Figure 6b encapsulates this result by showing the composite of all 1-point correlation maps based on grid boxes where $r_0 > 0.3$. The composite was constructed by averaging the correlation fields on a region of 90° of latitude and 180° of longitude centered in the reference grid box. The individual correlation field was shifted upside-down for reference grid boxes in the SH.

Actual (observed) geopotential anomalies lasting a month or longer are generally associated with global or hemispheric scale phenomena (e.g., ENSO, annular modes) and tend to exhibit a spatial extent larger than those shown in Fig. 6b. Nevertheless, global/hemispheric anomalies might be able to produce significant rainfall anomalies, provided that the largest zonal flow perturbations take place over regions where the local correlation between P and U_{300} is high.

Let us consider, for instance, the precipitation anomalies induced by the NH and SH annular modes (Thompson and Wallace 2000). Both modes are described as a seesaw of mass between the polar ice cap and midlatitudes, thus leading to marked mid- and upper-tropospheric zonal wind anomalies centered at about 60° and 35° of latitude. The temporal variability in the strength of these modes is quantified using the Arctic and Antarctic Oscillation Index[1] (AOI and AAOI, respectively). Figure 7a (7b) shows the correlation between AOI (AAOI) and monthly anomalies of CMAP precipitation and 300 hPa winds for the NH (SH). The annular modes does lead to significant rainfall anomalies on the relevant hemisphere (see also Jones and Widmann 2003; Holland 2003), with the largest positive (negative) anomalies at high (mid-) latitudes where

[1]Monthly AOI (AAOI) were obtained from CPC-NCEP from January 1979 to December 2004. They are constructed by projecting the monthly mean 1000-hPa (700-hPa) height anomalies onto the leading EOF mode of the monthly mean 1000-hPa (700-hPa) height anomalies poleward of 20° latitude for the Northern (Southern) Hemisphere. Both time series are normalized by the standard deviation of the monthly index (1979-2000 base period).

westerlies (easterlies) anomalies prevail in the upper troposphere. The AOI-P and AAOI-P correlation fields, however, exhibit an important zonally asymmetric component mostly explained by the spatial variability of the $U_{300} - P$ correlation field.

5 Concluding remarks

In this short contribution we have documented the covariability of the extratropical precipitation and circulation at seasonal, intraseasonal (month-to-month) and interannual time-scales, as well as the spatial correspondence between these variables when considering their climatological annual and seasonal means. While the emphasis of this work has been put on the local covariability, we also explored the large-scale circulation patterns that are best related with local precipitation anomalies. The key findings are as follow:

- The *spatial distribution* of the annual long-term-mean precipitation and upper-level zonal flow tends to agree over the extratropics, as precipitation maxima are often underneath the jet streams. Overall, the spatial variability of U_{300} explains nearly 40% of the spatial variability of P. The correspondence between precipitation and the variance of the upper-level meridional wind (a simple measure of the eddy-activity) is somewhat weaker, perhaps as a result of the more noisy structure of the variance field. The correspondence between precipitation and circulation is better in the NH relative to the SH, indicative of tighter coupling between upper level flow and precipitation in the NH.

- The local correlation between *monthly anomalies* of precipitation and upper-level zonal flow is significant over most of the extratropical oceans. In the NH the largest values ($r_0 > 0.5$) are found on the eastern side of the ocean basins; in the SH the largest values are found on a midlatitude circumglobal belt, as well as over the subtropical SPCZ and SACZ. Similar results are found when considering the monthly variance of the 300 hPa meridional winds as well as when performing the analysis with annual means.

- The significant, positive correlation between U_{300} and P over the midlatitude oceans and adjacent continental areas is consistent with the fact that strong westerlies aloft are conducive of a rapid growth and fast succession of baroclinic disturbances, leading to an increase of cyclone/frontal precipitation. The increase in local correlation near the western seabords of the continents and major mountain ranges seems associated with orographic effects superimposed on baroclinic storms.

- The orographic effects show up even more clearly in the local correlation map between precipitation and low-level (850 hPa) zonal flow. The correlations are positive and large upstream of the major meridionally-oriented

mountain ranges (e.g., the southern Andes), as stronger westerlies enhance upslope rain in addition to storm-related precipitation. In contrast, the correlation tends to be negative downstream of the ranges, as strong westerlies enhance the rain shadow effect over the lee side.

A variety of long-lasting, large-scale pressure patterns are able to disrupt the zonal flow aloft (e.g., ENSO, annular modes), leading to significant rainfall anomalies provided that the largest zonal flow perturbations take place over regions where the local correlation between P and U_{300} is significant. Thus, the local covariability between precipitation and circulation described in this paper provides a simple, yet efficient, framework to connect *large-scale* circulation anomalies with *regional-scale* precipitation anomalies, suitable for studies of past, present and future climate variability.

References

Adler, R., G.J. Huffman, A. Chang, R. Ferraro, P.P. Xie, J. Janowiak, B. Rudolf, U. Schneider, S. Curtis, D. Bolvin, A. Gruber, J. Susskind, P. Arkin and E. Nelkin, 2003: The Version-2 Global Precipitation Climatology Project (GPCP) Monthly Precipitation Analysis (1979-Present). *J. Hydrometeor.*, **4**, 1147-1167.

Eckhardt, S., A. Stohl, H. Wernli, P. James, C. Forster and N. Spichtinger, 2004: A 15-Year Climatology of Warm Conveyor Belts. *J. Climate*, **17**, 218-237.

Chang, E.K., S. Lee and K.L. Swanson, 2002: Storm Track Dynamics. *J. Climate*, **15**, 2163-2183.

Chang, E.K. and Y. Fu., 2002: Interdecadal Variations in Northern Hemisphere Winter Storm Track Intensity. *J. Climate*, **15**, 642-658.

Chen. T-S., W. Huang and E.S. Takle, 2004: Annual Variation of Midlatitude Precipitation. *J. Climate*, **17**, 4291-4298.

Frederiksen, J.S. and C.S. Frederiksen, 1993: Southern Hemisphere Storm Tracks, Blocking, and Low-Frequency Anomalies in a Primitive Equation Model. J. Atmos. Sci., **50**, 3148-3163.

Holland, M.M., 2003: The North Atlantic OscillationArctic Oscillation in the CCSM2 and Its Influence on Arctic Climate Variability. *J. Climate*, **16**, 2767-2781.

Hoskins, B.J. and P.J. Valdes, 1990: On the Existence of Storm-Tracks. *J. Atmos. Sci.*, **47**, 1854-1864.

Hoskins, B.J. and K.I. Hodges, 2002: New Perspectives on the Northern Hemisphere Winter Storm Tracks. *J. Atmos. Sci.*, **59**, 1041-1061.

Jones, J. and M. Widmann, 2003: Instrument- and Tree-Ring-Based Estimates of the Antarctic Oscillation. *J. Climate*, **16**, 3511-3524.

Nakamura, H., 1992: Midwinter Suppression of Baroclinic Wave Activity in the Pacific. *J. Atmos. Sci.*, **49**, 1629-1642.

Nakamura, H., T. Izumi and T. Sampe, 2002: Interannual and Decadal Modulations Recently Observed in the Pacific Storm Track Activity and East Asian Winter Monsoon. *J. Climate*, **15**, 1855-1874.

Nakamura, H. and A. Shimpo, 2004: Seasonal Variations in the Southern Hemisphere Storm Tracks and Jet Streams as Revealed in a Reanalysis Dataset. *J. Climate*, **17**, 1828-1844.

Paciorek, C.J, J.S. Risbey, V. Ventura and R.D. Rosen, 2002: Multiple Indices of Northern Hemisphere Cyclone Activity, Winters 194999. *J. Climate*, **15**, 1573-1590.

Pandey, G. R., D. R. Cayan, M. D. Dettinger, and K. P. Georgakakos, 2000: A hybrid model for interpolating daily precipitation in the Sierra Nevada of California during winter. *J. Hydrometeor.*, **1**, 491-506.

Renwick, J., 2005: Persistent Positive Anomalies in the Southern Hemisphere Circulation. *Mon. Wea. Rev.*, **133**, 977-988.

Roe G. H., 2005: Orographic Precipitation. *Annu. Rev. Earth. Planet. Sci.*, 33, 645-671

Thompson, D.W.J. and J.M. Wallace, 2000: Annular Modes in the Extratropical Circulation. Part I: Month-to-Month Variability. *J. Climate*, **13**, 1000-1016.

Trenberth, K.E., 1991: Storm tracks in the Southern Hemisphere. *J. Atmos. Sci.*, **48**, 2159-2178.

Xie, P. and P.A. Arkin, 1997: Global Precipitation: A 17-Year Monthly Analysis Based on Gauge Observations, Satellite Estimates, and Numerical Model Outputs. *Bull. Amer. Meteor. Soc.,* **78**, 2539 2558.

Yin, X., A. Gruber and P. Arkin, 2004: Comparison of the GPCP and CMAP Merged GaugeSatellite Monthly Precipitation Products for the Period 1979-2001. *J. Hydrometeor.*, **5**, 1207-1222.

Yoon, JH. and T. Chen, 2006: Maintenance of the Boreal Forest Rainbelts during Northern Summer. *J. Climate*, **19**, 1437-1449.

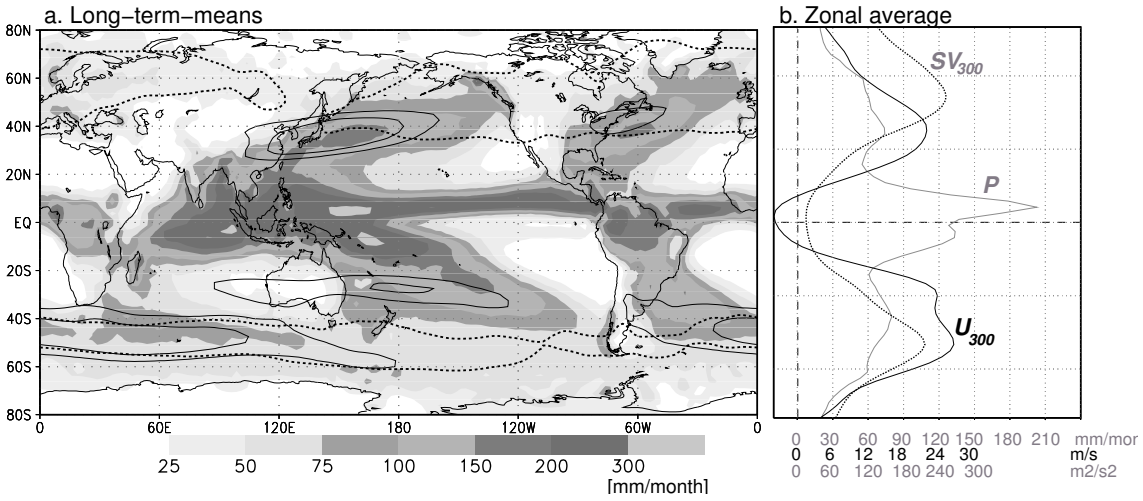

Figure 1. (a) Long-term (1979-2004) annual mean of CMAP precipitation (shaded, scale at the bottom), 300 hPa zonal wind (solid line, contours are 25 and 32 m/s), and variance of the band-pass-filtered (3-15 days) 300 hPa meridional wind (dotted line, contour is 200 m^2/s^2). The variance was calculated for each calendar month using daily values, and then averaged using all months. (b) Zonal average (0-360°) of the long term annual means: precipitation (solid, gray line), 300 hPa zonal wind (solid, black line), and variance of the band-pass-filtered (3-15 days) 300 hPa meridional wind (dotted line).

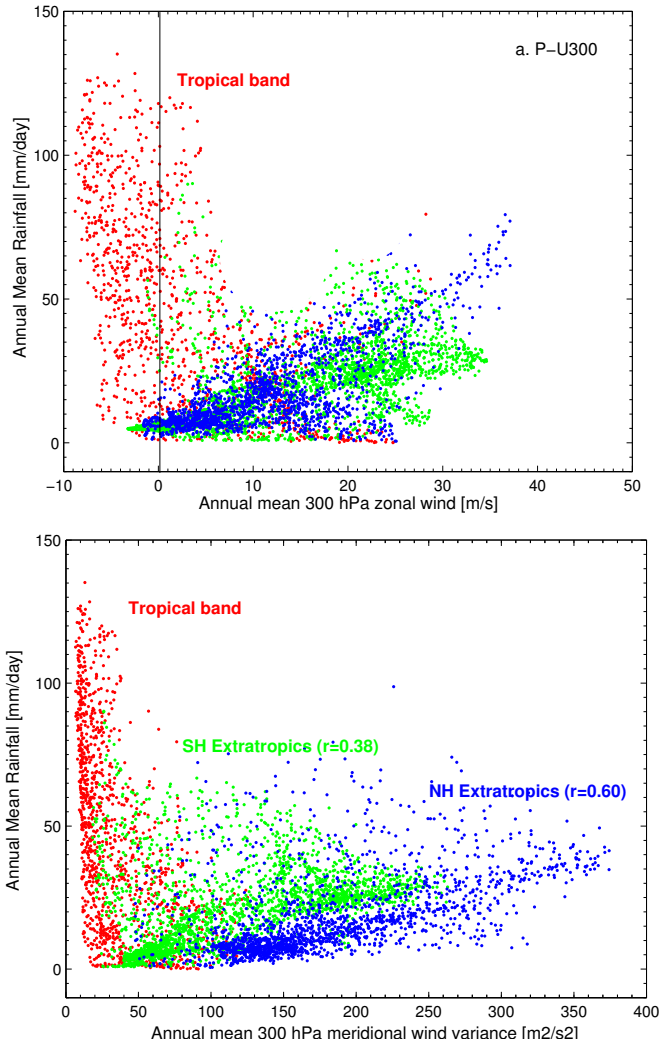

Figure 2. (a) Scatter plot of long-term annual mean precipitation and 300 hPa zonal wind at collocated grid boxes. Blue dots: grid boxes in the NH extratropics (25°-80°N); green dots: grid boxes in the SH extratropics (25°-80°S); red dots: grid boxes in the tropical belt (25°S-25°N). (b) As panel (a) but using the variance of the band-pass-filtered (3-15 days) 300 hPa meridional wind.

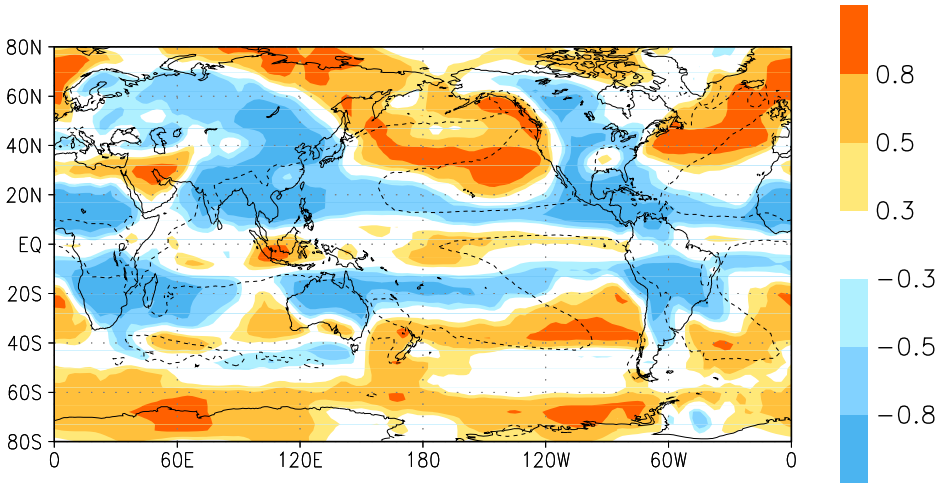

Figure 3. Map of local correlation (r_0) between precipitation and 300 hPa zonal wind using long-term (1979-2004) monthly means. Dashed lines outline regions where annual mean precipitation exceeds 1000 mm/year.

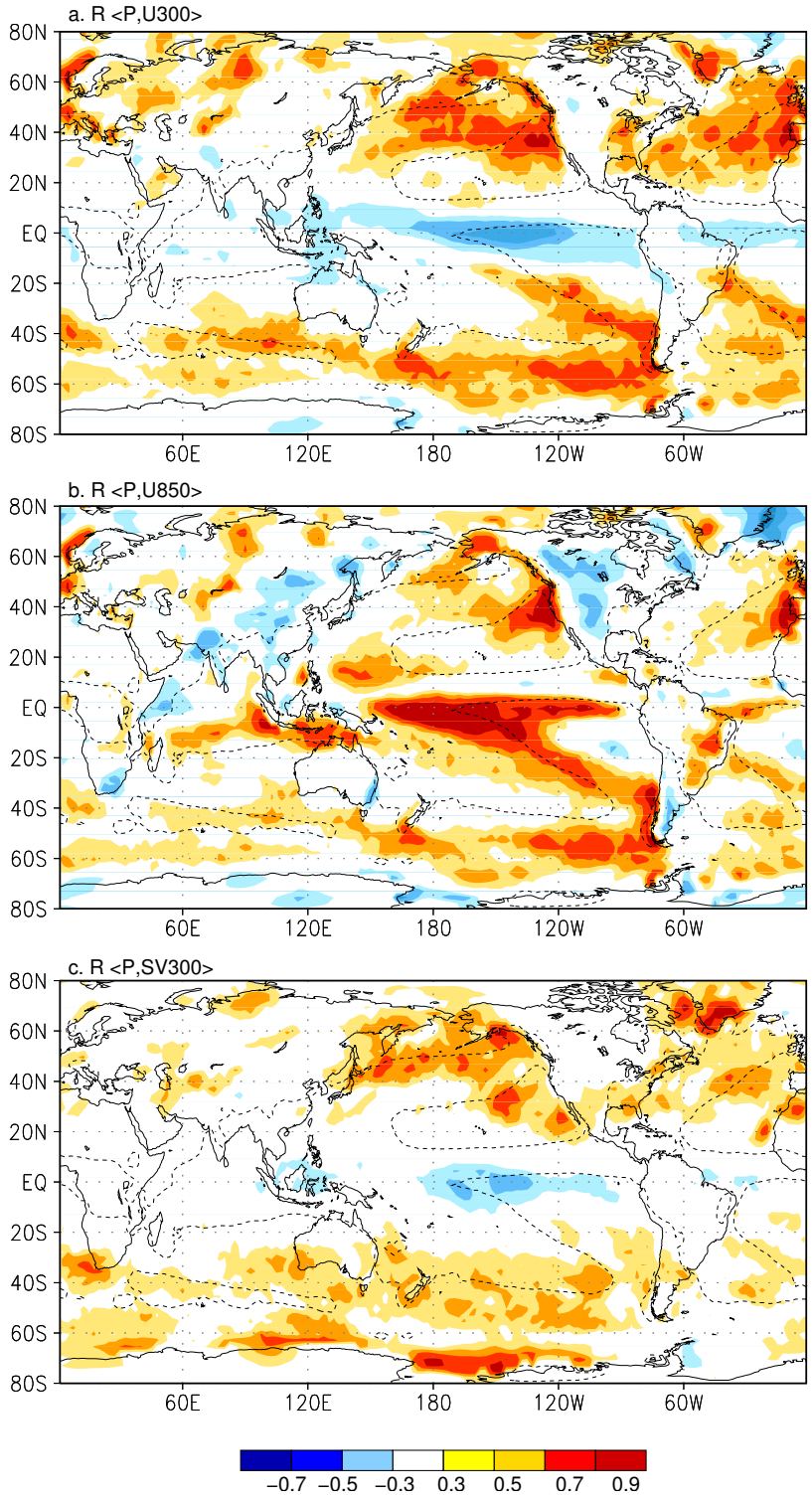

Figure 4. (a) Maps of local correlation between monthly anomalies of precipitation and 300 hPa zonal wind. Scale at the bottom. Dashed lines outline regions where annual mean precipitation exceeds 1000 mm/year. (b) As (a) but for local correlation between monthly anomalies of precipitation and 850 hPa zonal wind. (c) As in (a) but for local correlation between monthly anomalies of precipitation and variance of 300 hPa meridional wind.

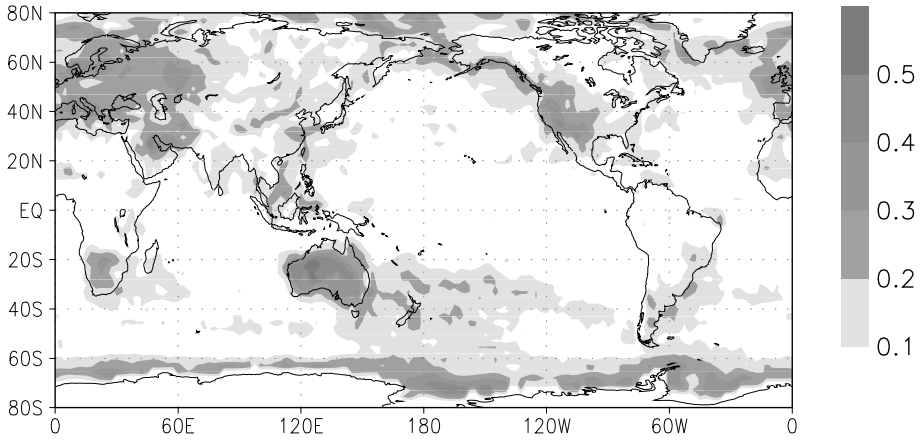

Figure 5. Increase in variance of precipitation (P) explained by a linear fit using 850 hPa zonal wind and relative humidity as predictors of P, relative to the case in which only the zonal wind is used. See text for further details.

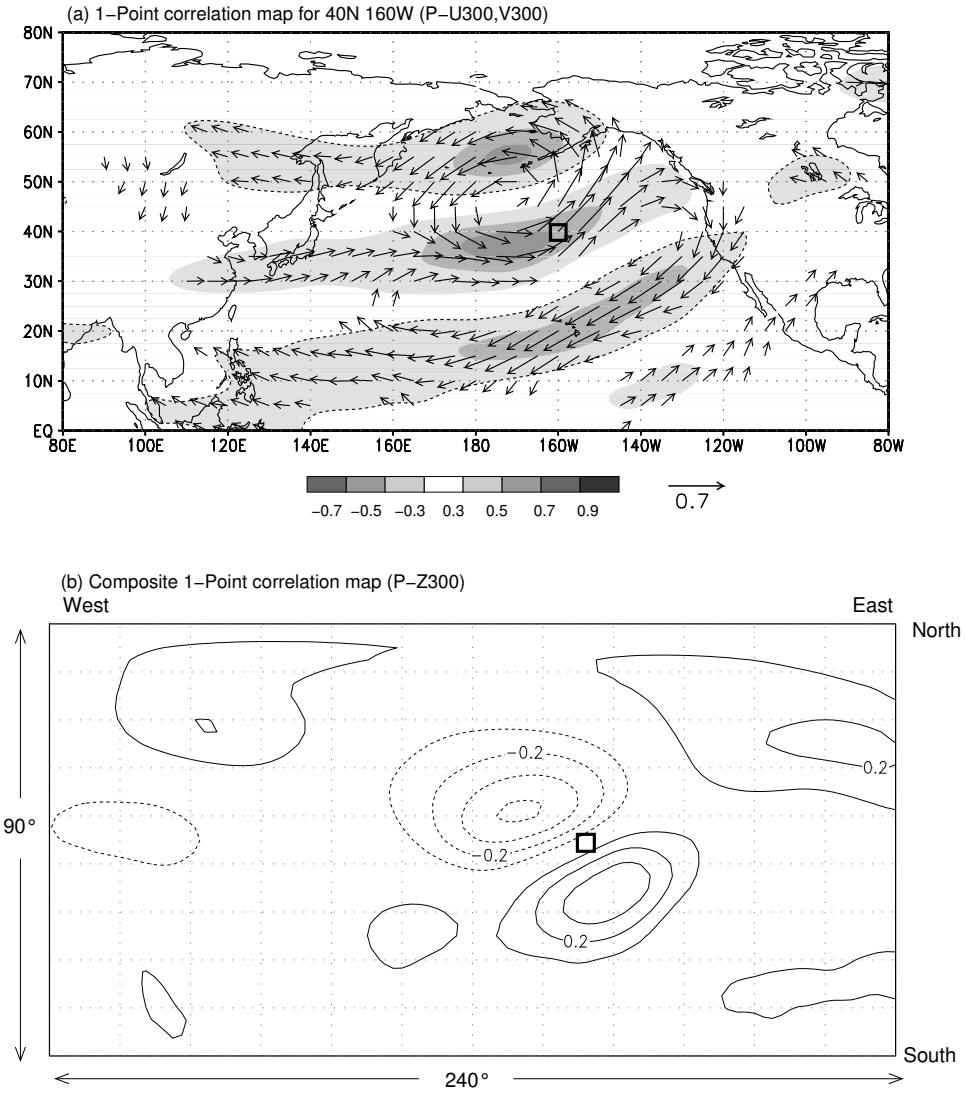

Figure 6. (a) Correlation between monthly anomalies of precipitation (P) over the central North Pacific (40°N, 160°W; grid box signaled by the thick square) and 300 hPa wind elsewhere. Shading indicates the correlation between P and 300 hPa zonal flow (dashed lines outline regions where $r_0 < 0$). Arrows indicate the correlation between P and 300 hPa wind vectors. Only vectors statistically significant at the 95% are shown. (b) Composite of 1-Point correlation maps between monthly anomalies of precipitation and 300 hPa geopotential height elsewhere. Contour interval is 0.1, negative values in dashed lines, and the zero line is omitted. See text for further details.

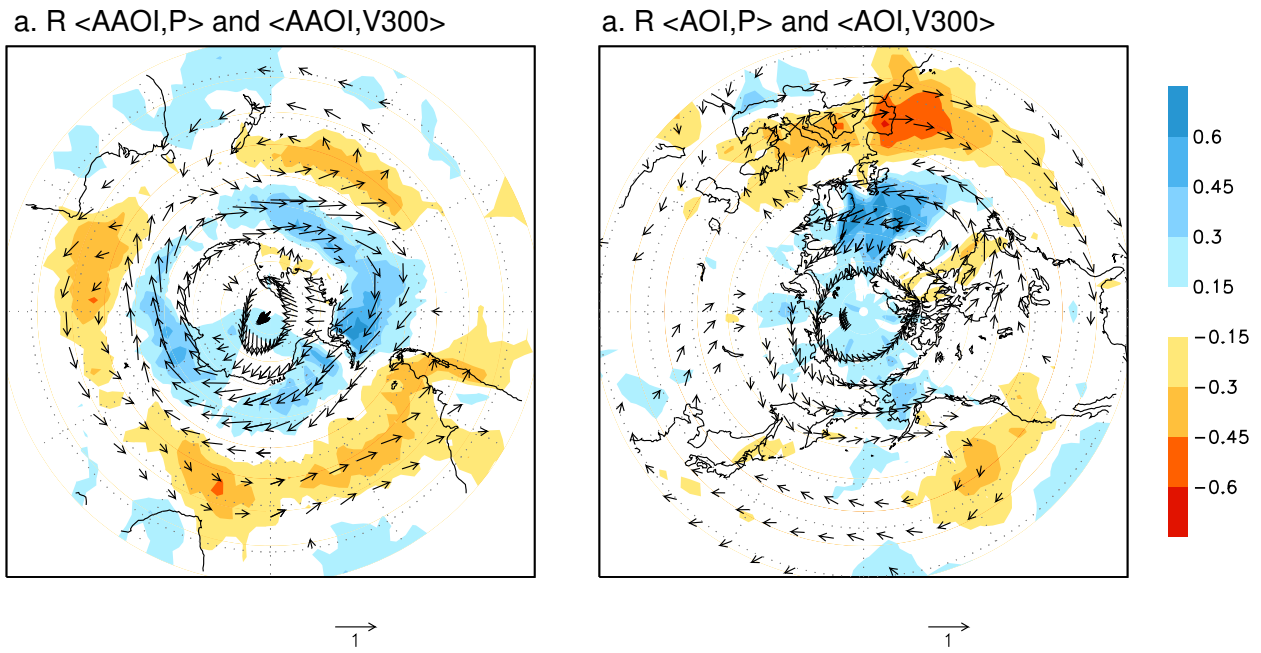

Figure 7. (a) Correlation coefficient between the monthly values of the Antarctic Oscillation Index (AAOI) and 300 hPa winds (arrows) and precipitation (shaded) for the SH. (b) As (a) but for the Arctic Oscillation Index (AOI) and the NH. Only vectors statistically significant at the 95% are shown.